

Cite this: *Dalton Trans.*, 2024, **53**, 12128

## Square-planar imido complexes of cobalt: synthesis, reactivity and computational study†

Jackson A. Reyna,<sup>a</sup> V. Mahesh Krishnan,<sup>†a</sup> Roberto Silva Villatoro,<sup>a</sup> Hadi D. Arman,<sup>a</sup> Sebastian A. Stoian,<sup>†b</sup> and Zachary J. Tonzetich<sup>†\*a</sup>

Treatment of [Co(N<sub>2</sub>)(<sup>t</sup>BuPNP)] (<sup>t</sup>BuPNP = anion of 2,5-bis(di-*tert*-butylphosphinomethyl)pyrrole) with one equivalent of an aryl azide generates the four-coordinate imido complexes [Co(NAr)(<sup>t</sup>BuPNP)] (Ar = mesityl, phenyl, or 4-*t*-Bu-phenyl). X-ray crystallographic analysis of the compounds shows an unusual square-planar geometry about cobalt with nearly linear imido units. In the presence of the hydrogen atom donor, TEMPOH, [Co(NPh)(<sup>t</sup>BuPNP)] undergoes addition of the H atom to the imido nitrogen to generate the corresponding amido complex, [Co(NHPh)(<sup>t</sup>BuPNP)], whose structure and composition were verified by independent synthesis. Despite the observation of H atom transfer reactivity with TEMPOH, the imido complexes do not show catalytic activity for C–H amination or aziridination for several substrates examined. In the case of [Co(NPh)(<sup>t</sup>BuPNP)], addition of excess azide produced the tetrazido complex, [Co(N<sub>4</sub>Ph<sub>2</sub>)(<sup>t</sup>BuPNP)], whose bond metrics were most consistent with an anionic Ph<sub>2</sub>N<sub>4</sub> ligand. Density Functional Theory (DFT) investigations of the imido and tetrazido species suggest that they adopt a ground state best described as possessing a low-spin cobalt(II) ion ferromagnetically coupled to an iminyl radical.

Received 20th May 2024,  
Accepted 24th June 2024

DOI: 10.1039/d4dt01483a

rsc.li/dalton

## Introduction

Transition metal-catalyzed nitrene addition/insertion is among the most desirable methods for construction of carbon–nitrogen bonds due to its atom economy and compatibility with late stage functionalization.<sup>1</sup> Several catalyst systems have proven successful in this regard demonstrating the ability to aminate C–H bonds with high efficiency and selectivity.<sup>2–4</sup> Azides are among the molecules most frequently employed as the source of nitrene units in these reactions as their conversion to C–N bonds results in molecular nitrogen as the only by-product. The reaction of organic azides with transition metal centres proceeds *via* oxidative group transfer of the “NR” fragment to generate metal-imido species.<sup>5</sup> The electronic structures of these compounds are often key to their ability to activate C–H bonds. Accordingly, early-metal imido complexes, which feature metals in high formal oxidation states and closed-shell NR<sup>2–</sup> ligands, are usually eschewed in favour of

later metal systems that may feature more electronic flexibility in the M–NR unit.<sup>6–12</sup>

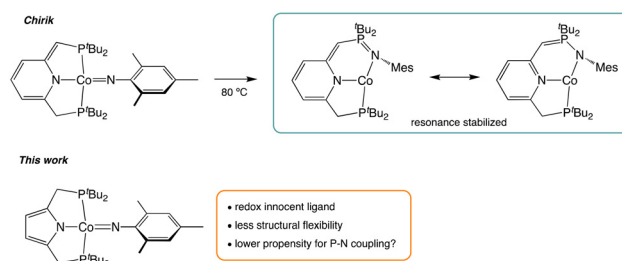
In the area of first-row transition metal chemistry, several compounds of the mid-to-late transition elements have been reported to support well-defined metal imido species while also demonstrating catalytic efficacy in amination protocols.<sup>13</sup> Cobalt, in particular, has proven promising as a focal point for further catalyst design with several systems displaying both efficiency and selectivity for C–H amination.<sup>14–19</sup> In this vein, recent work with a cobalt PNP pincer system by Chirik and co-workers disclosed one of the first examples of an isolable imido complex possessing a square-planar geometry (Scheme 1).<sup>20</sup> The compound was prepared by treatment of a cobalt(I) dinitrogen complex with mesityl azide. As noted by the authors, such geometries are rare for species containing metal–ligand multiple bonds. Moreover, the ground state for

<sup>a</sup>Department of Chemistry, University of Texas at San Antonio (UTSA), San Antonio, TX 78249, USA. E-mail: zachary.tonzetich@utsa.edu<sup>b</sup>Department of Chemistry, University of Idaho, Moscow, ID 83844, USA.

E-mail: sstoian@uidaho.edu

† Electronic supplementary information (ESI) available: NMR spectra; the cyclic voltammogram of **2a**; the EPR spectrum of **4a**; additional computational details, figures, and tables. CCDC 2334970–2334974. For ESI and crystallographic data in CIF or other electronic format see DOI: <https://doi.org/10.1039/d4dt01483a>

‡ Present address: Eastman Chemical Company, 200 S. Wilcox Dr., Kingsport, TN 37660.



Scheme 1 Pincer-supported Co imido complexes.

the imido was found to be best described as a low-spin Co(II) centre ferromagnetically coupled to an iminyl radical giving an overall ground state of  $S = 1$ . Despite this unusual electronic structure, the imido proved unreactive in typical nitrene transfer protocols and instead was found to decompose by migration of the nitrene unit to one of the phosphine ligands. The resulting cobalt(I) species was computed to be stabilized by *ca.* 9 kcal mol<sup>-1</sup> by resonance contributions from the non-innocent PNP ligand (Scheme 1).

Encouraged by the precedent of cobalt compounds in nitrene chemistry<sup>21–32</sup> and the demonstrated ability of pincer ligands to support novel metal imido species,<sup>33–38</sup> we turned our focus to the chemistry of the Co(I) compound featuring the pyrrole-based pincer ligand (Scheme 1).<sup>39,40</sup> We have already established the propensity for this species to carry out two-electron oxidative addition reactions with concomitant bond activation. Accordingly, we hypothesized that the corresponding reactions with azides would generate similar imido species to those reported by Chirik, but with a ligand that would not be as prone to formation of the P–N coupling product due to the lack of possible resonance contributors with the pyrrole-based pincer ligand and its greater structural rigidity. We describe our findings herein.

## Results and discussion

### Synthesis

We have demonstrated previously that the Co(I) species, [Co(N<sub>2</sub>)(<sup>R</sup>PNP)] (R = Cy, <sup>t</sup>Bu), is capable of H–H, C–H, C–X, and Si–H bond activation under mild conditions.<sup>41–43</sup> These reactions occur *via* formal oxidative addition to generate Co(III) species. We therefore reasoned that the reducing potential of the Co(I) complex would be similarly effective for activation of organic azides. Treatment of the *tert*-butyl analogue, **1**, with mesityl azide was found to proceed rapidly at room temperature with the evolution of nitrogen to produce a new paramagnetic species formulated as the formally cobalt(III) imido species, **2a** (Scheme 2), as determined by NMR spectroscopy. The solution

magnetic susceptibility measurements of the compound in benzene provided a magnetic moment of 2.6(2) $\mu_B$ . This value is low but most consistent with a triplet ground state ( $S = 1$ ). Identical reactions of phenyl azide and 4-*tert*-butylphenyl azide generated comparable spectra although alkyl azides such as benzyl azide led to intractable mixtures. The bulkier alkyl azide 1-AdN<sub>3</sub> failed to react with **1** under the conditions employed. Compound **2a** was found to precipitate readily from cold pentane to afford dark olive-green crystals. Slow degradation was observed in solution at room temperature with more rapid decomposition evident at 80 °C in benzene-*d*<sub>6</sub>.

The solid-state structure of **2a** is displayed in Fig. 1. The compound displays a square-planar coordination geometry about cobalt much like that found for the related PNP pincer system studied by Chirik and coworkers.<sup>20</sup> The cobalt imido distance of 1.728 Å is nearly 0.2 Å shorter than the Co–N<sub>pyrrole</sub> contact indicating a degree of cobalt–nitrogen multiple bonding consistent with the imido formulation. In addition, the Co(1)–N(2)–C(23) angle is very close to linear at 178.2°. Within the mesityl ring, the C–C distances are not equivalent, with the C<sub>ipso</sub>–C<sub>ortho</sub> distances measuring *ca.* 0.05 Å longer than the remaining bonds. Similar elongation has been observed previously for transition metal imido species containing radical delocalisation into the pi system.<sup>44–47</sup> The structure of the phenyl analogue, **2b**, is similar to that of **2a** with a slightly more bent Co–N–C angle of 155.2° (see the ESI†). The deviation from linearity is likely made possible by the reduced steric congestion encountered by the smaller phenylimido ligand. Cobalt arylimido complexes are known to display a range of Co–N–C angles, with that in **2b** falling at the lower end of structurally characterized examples.<sup>21</sup> Nonetheless, this angle is substantially more linear than that found for the amido analogue (*vide infra*).

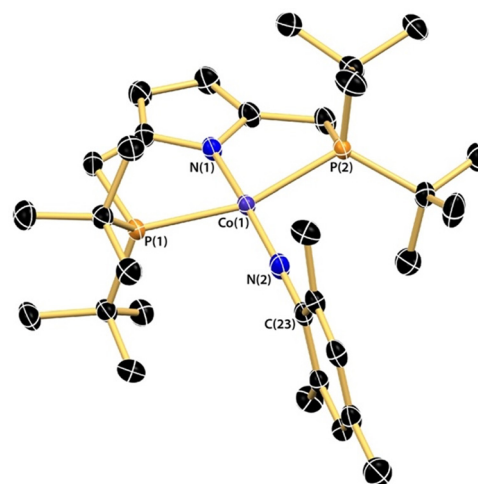
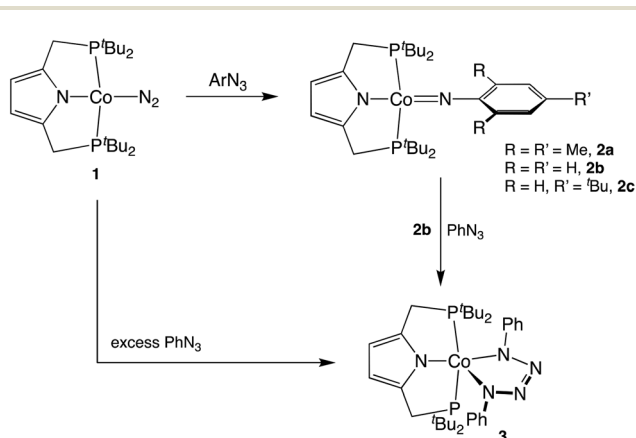


**Fig. 1** Thermal ellipsoid drawing of the solid-state structure of **2a**. Hydrogen atoms omitted for clarity. Selected bond distances (Å) and angles (°): Co(1)–N(2) = 1.7278(14); Co(1)–N(1) = 1.8922(14); Co(1)–P(1) = 2.2549(4); Co(1)–P(2) = 2.2521(4); N(2)–C(23) = 1.334(2); Co(1)–N(2)–C(23) = 178.25(13); P(1)–Co(1)–P(2) = 161.654(19); N(1)–Co(1)–N(2) = 169.90(7).



**Scheme 2** Azide reactivity of [Co(N<sub>2</sub>)(<sup>t</sup>BuPNP)].

Cyclic voltammetry of **2a** in THF demonstrated a quasi-reversible oxidation centred at  $-0.60$  V (vs.  $\text{Fc}^{+/0}$ ) and an irreversible reduction event at  $-2.38$  V (see the ESI†). Attempted chemical oxidation of **2a** with ferrocenium salts generated a deep red material that appeared silent in NMR spectroscopy; however, attempts to isolate the material for further characterization were unsuccessful.

During the synthesis of **2b**, prolonged reaction with excess phenylazide was found to produce a new compound as studied by NMR spectroscopy. Crystallization of the species and analysis by X-ray diffraction demonstrated the formation of a tetrazido complex (**3**, Scheme 2), congruent with observations from other metal imido systems.<sup>15,44,48</sup> Compound **3** features a distorted square-pyramidal geometry in the solid state with one of the tetrazido nitrogen atoms occupying the axial position (Fig. 2). The  $^1\text{H}$  NMR spectrum of **3** contains a single broad resonance for the *tert*-butyl groups indicating a fluxional geometry in solution with the  $\text{N}_4$  moiety likely rocking back and forth about the PNPCo plane. The bond distances within the  $\text{N}_4$  metallacycle vary between  $1.35$  Å for N(2)–N(3) and N(4)–N(5), and  $1.29$  Å for N(3)–N(4). This shortening of the central N–N contact is most consistent with a ‘closed-shell dianionic’ description of the tetrazido moiety ( $\text{N}_4^{2-}$ ),<sup>49</sup> although calculations of **3** suggest a multi-determinantal ground state (*vide infra*). Similar tetrazido formation was not observed for **2a**, probably because of the enhanced steric bulk of the mesityl substituents. In addition, a species analogous to **3** was not observed by Chirik for the pyridine-based PNP system containing a mesitylimido moiety.<sup>20</sup>

Hydrogen atom abstraction by metal imido species is commonly invoked as an initial step in the mechanism for catalytic

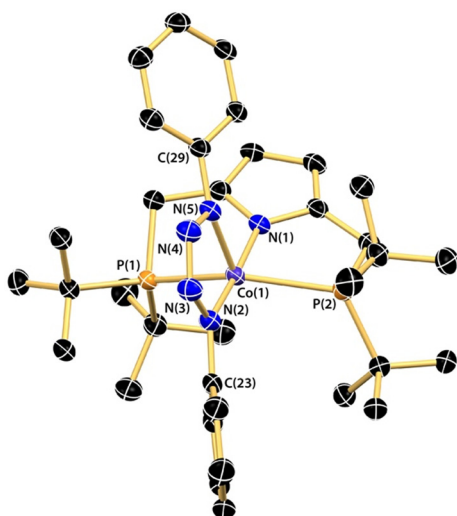


Fig. 2 Thermal ellipsoid drawing of the solid-state structure of **3**. Hydrogen atoms omitted for clarity. Selected bond distances (Å) and angles (°): Co(1)–N(2) = 1.8772(18); Co(1)–N(5) = 1.9650(19); Co(1)–N(1) = 1.9090(18); Co(1)–P<sub>avg</sub> = 2.3904(6); N(2)–N(3) = 1.354(3); N(3)–N(4) = 1.288(3); N(4)–N(5) = 1.359(2); P(1)–Co(1)–P(2) = 146.23(2); N(1)–Co(1)–N(2) = 175.74(8); N(1)–Co(1)–N(5) = 97.45(7); N(2)–Co(1)–N(5) = 78.30(8).

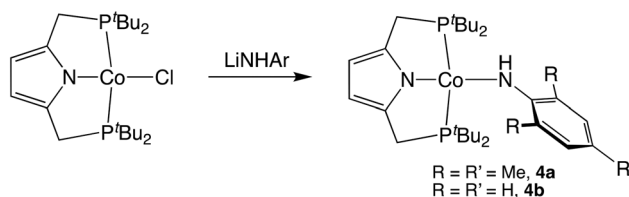
C–H amination.<sup>50</sup> To provide a benchmark for spectroscopic features of such species we next pursued the synthesis of the Co(II) amido species, **4** (Scheme 3). Addition of LiNAr salts to  $[\text{CoCl}(\text{t}^{\text{Bu}}\text{PNP})]$  afforded the desired amido compounds in moderate isolated yields.

Compounds **4a** and **4b** precipitate readily from pentane to afford deep purple crystals. The EPR spectrum of **4b** displays a pseudo-axial signal with hyperfine coupling to  $^{57}\text{Co}$ . These features are broadly similar to those of other low-spin  $S = \frac{1}{2}$  cobalt (II) compounds of PNP pincers containing alkyl and halogen ligands (Fig. 3).<sup>51</sup> Simulation of the spectrum produced anisotropic  $g$  values of 3.288, 1.994, and 1.853, further consistent with a low-spin square-planar Co(II) system displaying substantial spin–orbit coupling.<sup>51–53</sup> In line with this spectroscopic data, the effective magnetic moment of **4a** in solution was determined to be  $2.2(2)\mu_{\text{B}}$ , greater than the predicted spin-only value for an  $S = \frac{1}{2}$  system.

The solid-state structure of **4a** is depicted in Fig. 4. Most notably, the bond metrics about the cobalt-amido unit show a substantial change from those observed for the cobalt-imido unit of compound **2a**. The Co(1)–N(2) bond distance of **4a** is over  $0.1$  Å longer than that in **2a** at  $1.875$  Å. Similarly, the Co(1)–N(2)–C(23) bond angle of **4a** is significantly more bent at  $135.45^\circ$ . In addition to the metrics about Co, the C–C intraring distances of the mesityl unit and the N(2)–C(23) distance demonstrate less deviation from normality than seen in **2a** consistent with less radical delocalization into the arene pi system. The remaining metrics about the CoPNP unit are comparable to those of **2a** with the exception of the Co(1)–P(2) distance, which is slightly elongated with respect to the Co(1)–P(1) distance. This distortion most likely takes place to accommodate the bulk of the amido substituent, as it is also observed in the structure of **4b** (see the ESI†).

## Reactivity

With the imido compounds in hand, we turned to an investigation of their reactivity relevant to C–H amination processes. We began by examining the propensity for hydrogen atom abstraction by **2a**. Reaction of **2a** with H atom donors, 1,4-cyclohexadiene or TEMPOH (2,2,6,6-tetramethylpiperidin-1-ol) in benzene- $d_6$  resulted in no apparent reactivity as judged by  $^1\text{H}$  NMR spectroscopy. Resonances for **2a** were still apparent after prolonged exposure to the H atom donors and extended reaction time and/or elevated temperatures led to decomposition. Reasoning that the steric bulk of **2a** was shutting down potential HAT reactivity, we next examined compound **2b**.



Scheme 3 Synthesis of Co(II) amido species.

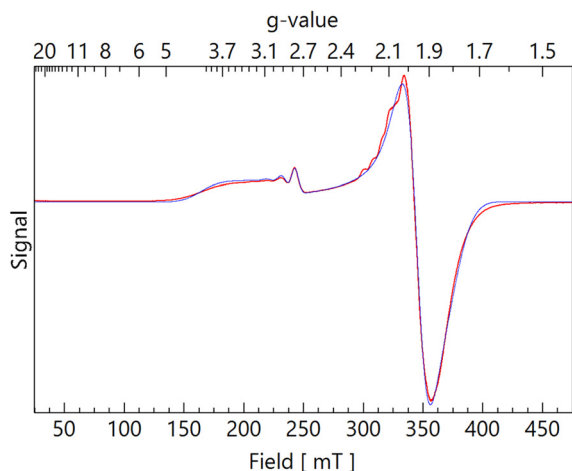


**Fig. 3** X-band EPR spectrum recorded at 77 K for a 2-MeTHF solution of **4b** (red) recorded at a microwave frequency of  $\nu = 9.44869$  GHz and a microwave power of 2 mW. The theoretical spectrum (blue) was obtained using a model consisting of an  $S = \frac{1}{2}$  coupled to a  $I = \frac{7}{2}$   $^{59}\text{Co}$  nucleus (100% abundance). The parameters used to derive this simulation are  $g_x = 3.288$ ,  $g_y = 1.994$ ,  $g_z = 1.853$ ,  $\sigma(g_x) = 0.077$ ,  $\sigma(g_y) = 0.046$ ,  $\sigma(g_z) = 0.071$ ,  $A_x = 489$  MHz,  $A_y = 5$  MHz,  $A_z = 29$  MHz,  $\sigma(A_x) = 120$  MHz,  $\sigma(A_y) = 51$  MHz,  $\sigma(A_z) = 2$  MHz and a linewidth of 57 G. Although the simulation was not able to reproduce the small ridges centered around  $g \sim 2.2$ , their peak-to-peak splitting suggests that they originate from a hyperfine splitting of ca. 210 MHz.

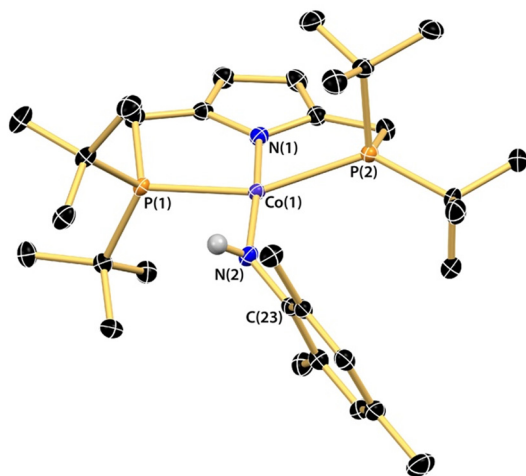


**Fig. 4** Thermal ellipsoid drawing of the solid-state structure of **4a**. Hydrogen atoms except that attached to N(2) omitted for clarity. Selected bond distances (Å) and angles ( $^\circ$ ): Co(1)–N(2) = 1.8750(15); Co(1)–N(1) = 1.8877(14); Co(1)–P(1) = 2.2626(5); Co(1)–P(2) = 2.3198(5); N(2)–C(23) = 1.395(2); Co(1)–N(2)–C(23) = 135.44(13); P(1)–Co(1)–P(2) = 158.022(19); N(1)–Co(1)–N(2) = 172.54(6).

Reaction of **2b** with 1,4-cyclohexadiene resulted in the detection of small quantities of aniline and **1** by NMR spectroscopy, although it remains uncertain if direct hydrogen atom transfer (HAT) to the imido nitrogen atom of **2b** occurred as no evidence for the formation of **4b** was observed.<sup>54</sup> In contrast,

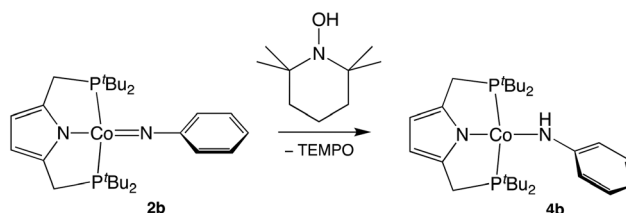
treatment of **2b** with TEMPOH led to the immediate formation of **4b** as judged by NMR spectroscopy (Scheme 4).

In addition to stoichiometric experiments with **2a** and **2b**, we also examined the potential catalytic activity of **1** with several typical amination substrates. Reactions of **1** with a 5–10 fold excess of styrene or toluene in the presence of phenyl and benzyl azides failed to demonstrate any reactivity consistent with nitrene transfer. In all cases complete consumption of **1** was observed, but no products indicative of C–N bond formation were apparent. We also considered intramolecular nitrene transfer employing the substrate (3-azidobutyl) benzene. As with the intermolecular experiments, treatment of **1** with an excess of the azide led to the immediate consumption of reagents but failed to produce the expected phenylpyrrolidine product as judged by NMR spectroscopy. These results demonstrate that imido formation is facile with the azide substrate, but that subsequent C–H abstraction and amination are not occurring, likely due to the decomposition or orthogonal reactivity of the intermediate alkylimido such as tetrazido formation.

### Computational studies

The electronic structures of the imido, amido and tetrazido complexes were investigated by performing a series of DFT and *ab initio* Complete Active Space Self Consistent Field (CASSCF) calculations on structural models derived from the crystal structures. DFT calculations employed pure BP86 and hybrid B3LYP and TPSSH functionals in conjunction with the Karlsruhe triple-zeta def2-TZVPP basis set.<sup>55</sup>

**Imido complexes.** The DFT calculations predict that the imido complex, **2a**, adopts a triplet ground state ( $S = 1$ ) consistent with experimental data. The lowest energy excited state sits ca. 1200  $\text{cm}^{-1}$  above the ground state and is best described as a broken symmetry (BS)  $S = 0$  state. The energy of the lowest genuine  $S = 0$  state is ca. 8000  $\text{cm}^{-1}$  above the ground state and was inferred from restricted Kohn–Sham calculations (rks). Moreover, the lowest quintet state ( $S = 2$ ) has similar energy as that of the rks  $S = 0$  state. Inspection of the DFT predicted atomic charges and spins (see the ESI<sup>†</sup>) shows that the two unpaired electrons of the lowest  $S = 0$ , BS state and of the  $S = 1$  ground state are nearly equally distributed between the cobalt site and the imido ligand (Fig. 5). Evidently, for the BS state the electron localized on the ligand has an opposite spin when compared to that localized on the metal site. This observation suggests that the ground state may be described as orig-



**Scheme 4** HAT reactivity of **2b** with TEMPOH.

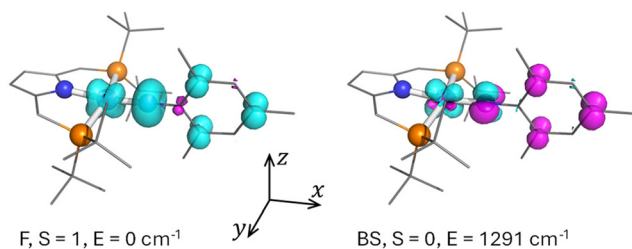


Fig. 5 Spin density plots of **2a** obtained for the F,  $S = 1$  states (left) and the BS,  $S = 0$  (right) obtained at the BP86/def2-TZVPP (left) level of theory. These plots were obtained using an isosurface value of  $\pm 0.008$ .

inating from the ferromagnetic (F) coupling of a metal-based  $S_{\text{Co}} = \frac{1}{2}$ , such as that obtained for a low-spin Co(II) site, with the  $S_{\text{imido}} = \frac{1}{2}$  of an imido-based spin.

The energy spacing of the F and BS states suggests a spin coupling constant of  $J \sim -2400 \text{ cm}^{-1}$ , obtained using the Hamiltonian,  $\hat{H} = J \hat{S}_{\text{Co}} \hat{S}_{\text{imido}}$  and the  $J = (\epsilon_{\text{F}} - \epsilon_{\text{BS}}) / 2S_{\text{Co}}S_{\text{imido}}$  relationship. Just as expected, the large  $J$  value is indicative of a direct exchange interaction as opposed to superexchange interactions encountered when the spin coupling is mediated by a diamagnetic bridge.

In the ferromagnetically coupled ground state of **2a** the unpaired spin density of the imido ligand is, in most cases, nearly equally distributed between the nitrogen atom and the aromatic core (Fig. 5). The delocalization of the unpaired electron over the latter moiety is consistent with the elongated C–C bonds of the aromatic ring, and likely accounts for the added stability of the arylimido compounds vis-a-vis alkylimidos. The unpaired spin density localized specifically on the nitrogen atom is accommodated by the  $2p_z$  and  $2p_y$  orbitals, which are orthogonal to the Co–N bond. The  $p_z$  fraction is typically twice as large as  $p_y$  (see the ESI†). This difference may be traced to the fact that only  $p_y$  interacts with the  $\pi$  system of the benzene core. Thus, the two unpaired electrons of both the F and BS states occupy two  $\pi^*$ -type MO orbitals:  $\pi_y^* \sim 3d_{xy}(\text{Co}) - [p_y(\text{N}_{\text{imido}}) + p(\text{C6})]$ ;  $\pi_z^* \sim 3d_{xz}(\text{Co}) - p_z(\text{N}_{\text{imido}})$  (see ESI Fig. S12†). Importantly, this difference leads to unequal contributions of the 3d cobalt orbitals to the ( $\pi_y^*$ ,  $\pi_z^*$ ) MOs and, in turn, is responsible for the stabilization of a ferromagnetic-type ground state.

Orbital occupation in the ground state of **2a** is best described as having single occupation of the  $3d_{xz}$  orbital with double occupancy of  $3d_{z^2}$ ,  $3d_{xy}$  and  $3d_{yz}$  (see the ESI†). The metal-based  $3d_{x^2-y^2}$  orbital also appears to accommodate one electron; however the population of this orbital is spin unpolarized and is traced to the  $\sigma$ -bonding interaction between the empty metal orbital and doubly occupied ligand orbitals. Therefore, the metal site is best described as a low-spin Co(II) ion. The increased  $\pi$ -bonding interaction is also reflected in a strong Co–N<sub>imido</sub> bond. Thus, the bond order calculated for this bond is nearly 1.5 times larger than the other metal–ligand bonds.

The CAS(8,12) calculations of **2a** also predict that there is a strong  $\pi$ -bonding interaction between the cobalt ion and the

imido ligand (see ESI, Fig. S13†). Unlike DFT, however, the CAS(8,12) calculations forecast that the two unpaired electrons are localized primarily on the metal ion such that, according to the Löwdin population analysis, the cobalt site has a spin density of +1.68 and the imido ligand of +0.22. In addition, these calculations suggest that the  $S = 1$  ground state exhibits an exceptionally large zero field splitting (ZFS),  $D \sim 92 \text{ cm}^{-1}$  with a large contribution from the singlet states of *ca.*  $51 \text{ cm}^{-1}$ . This  $D$  value is similar to that observed experimentally for a  $S = 1$ , square-planar Co(III) complex supported by perfluoropinacolates,<sup>56</sup> and could potentially explain our inability to detect an EPR signal for this species even when using a microwave frequency greater than 600 GHz ( $h\nu > 20 \text{ cm}^{-1}$ ).

**Amido complexes.** Analysis of the DFT predicted charge and spin distributions suggests that the lone unpaired electron of the  $S = \frac{1}{2}$  ground state of the amido complex **4a** is localized on the metal ion (see ESI, Fig. S14†). The lowest quartet excited state ( $S = \frac{3}{2}$ ) has an energy of *ca.*  $10\,000 \text{ cm}^{-1}$  above the ground state. Moreover, inspection of the orbital populations, indicates that the unpaired electron is accommodated in a  $3d_{xz}$  orbital with double occupation of  $3d_{z^2}$ ,  $3d_{xy}$  and  $3d_{yz}$  akin to that calculated for the low-spin Co(II) centre in **2a**. Therefore, the electronic configuration of the low-spin cobalt(II) ion of the amido complex is quite similar to that of the imido except that the  $\pi$ -bonding interactions between the metal site and the amido ligand are not as important.

**Tetrazido complex.** The DFT study of **3** suggests that the electronic structures of the tetrazido and imido species share many characteristics. Thus, DFT predicts a triplet ( $S = 1$ ) ground state that originates from the ferromagnetic coupling of a  $S = \frac{1}{2}$  low-spin cobalt(II) ion to the  $S = \frac{1}{2}$  spin delocalized over the N<sub>4</sub> moiety (Fig. 6 and the ESI†). In addition, the lowest excited state is a broken symmetry singlet ( $S = 0$ ) with an energy of  $\sim 900 \text{ cm}^{-1}$  ( $J \sim 1800 \text{ cm}^{-1}$ ). While the unpaired electron of the tetrazido ligand occupies a  $b_1$  molecular orbital delocalized over the N<sub>4</sub> moiety, that of the metal ion is best described as occupying  $3d_{z^2}$  (see ESI, Fig. S17†). The CAS(7,10) calculations predict that **3** adopts a multi-determinantal ground state with contributions from multiple leading configurations and that the unpaired electron is localized primar-

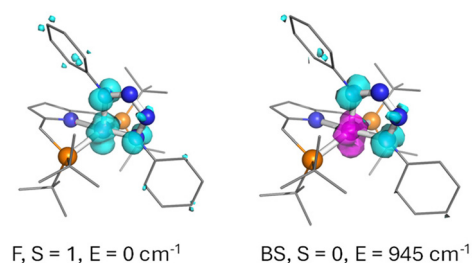


Fig. 6 Spin density plots of **3** obtained for the F,  $S = 1$  states (left) and the BS,  $S = 0$  (right) obtained at the BP86/def2-TZVPP (left) level of theory. The density plots were generated using an isosurface value of  $\pm 0.008$ .

ily on the metal ion (see ESI, Fig. S18†). Just as for the imido, these calculations suggest that the tetrazido complex exhibits a very large ZFS except that in this case the theoretical  $D$  is negative ( $D < -80 \text{ cm}^{-1}$ ).

## Conclusions

In conclusion, the Co(I) compound  $[\text{Co}(\text{N}_2)(^t\text{BuPNP})]$  has been found to serve as a precursor to aryl imido species of the type  $[\text{Co}(\text{NAr})(^t\text{BuPNP})]$  through treatment with organic azides. The imido species adopt rare square-planar geometries with bond distances indicative of radical delocalization into the aryl ring. Hydrogen atom transfer was observed in the case of the phenyl imido compound, but only with very active H atom donors. With the smaller phenylamido ligand, addition of two or more equivalents of azide was found to result in the formation of a tetrazido complex. Computational studies on the cobalt imido compounds indicate that the electronic structure is best regarded as arising from low-spin Co(II) centres ferromagnetically coupled to an iminyl radical. The strong ligand field engendered by the PNP ligand likely results in the low-spin configuration for cobalt and may explain the differential reactivity in comparison to other well-defined Co(III) imido complexes.

## Experimental

### General

Manipulations of air- and moisture-sensitive materials were performed under an atmosphere of purified nitrogen gas using a Vacuum Atmospheres glovebox. Tetrahydrofuran, diethyl ether, pentane, and toluene were purified by sparging with argon and passage through two columns packed with 4 Å molecular sieves and/or activated alumina (THF). Benzene- $d_6$  and toluene- $d_8$  were dried over sodium and vacuum-distilled prior to use. NMR spectra were recorded on a Varian INOVA spectrometer operating at 300 or 500 MHz ( $^1\text{H}$ ) and referenced to the residual protium resonance of the solvent. UV-Vis spectra were recorded on a Cary-60 spectrophotometer in airtight Teflon-capped quartz cells. Cyclic voltammetry was performed under purified nitrogen at 23 °C on a CH Instruments 620D electrochemical workstation. A three-electrode setup was employed, comprising a glassy-carbon working electrode, platinum-wire auxiliary electrode, and an Ag/AgCl quasi-reference electrode. Triply recrystallized  $\text{Bu}_4\text{NPF}_6$  was used as the supporting electrolyte. All electrochemical data were referenced internally to the ferrocene/ferrocenium couple at 0.00 V. Elemental analyses were performed by the CENTC facility at the University of Rochester.

### Materials

Compound **1** and  $[\text{CoCl}(\text{}^t\text{BuPNP})]$  were synthesized according to literature procedures or slight modifications thereof.<sup>57</sup> Aryl azides were prepared following published procedures with

strict adherence to recommended safety precautions.<sup>58</sup>  $\text{LiNHPH}$  and  $\text{LiNHMe}$ s were prepared by deprotonation of the corresponding anilines with *n*-butyllithium in pentane. All other materials were purchased from commercial sources and used as received.

### Crystallography

Crystals suitable for X-ray diffraction were mounted, using Paratone oil, onto a nylon loop. Data were collected at 98(2) K using a Rigaku AFC12/Saturn 724 CCD fitted with Mo  $K\alpha$  radiation ( $\lambda = 0.71075 \text{ \AA}$ ) or at 100.0(1) K using a Rigaku XtaLAB Synergy/Dualflex, HyPix fitted with Cu  $K\alpha$  radiation ( $\lambda = 1.54184 \text{ \AA}$ ). Data collection and unit cell refinement were performed using the CrysAlisPro software.<sup>59</sup> Data processing and absorption correction were accomplished with CrysAlisPro and SCALE3 ABSPACK,<sup>60</sup> respectively. The structure, using Olex2,<sup>61</sup> was solved with the ShelXT structure solution program using direct methods and refined (on  $F^2$ ) with the ShelXL refinement package using full-matrix, least-squares techniques.<sup>62,63</sup> All nonhydrogen atoms were refined with anisotropic displacement parameters. All hydrogen atom positions were determined by geometry and refined by a riding model. Crystallographic data and refinement parameters for each structure can be found in the ESI.†

### Computational studies

The electronic structures of **2a**, **3** and **4a,b** were investigated using Density Functional Theory (DFT) and *ab initio* Complete Active Space (CAS) Self Consistent Field (SCF) methods as implemented in the ORCA 5 quantum-chemical software package.<sup>64,65</sup> All calculations used the def2-TZVPP5,<sup>66</sup> basis set and the required auxiliary basis set were included using the autoaux keyword. In addition, resolution of identity (RI) approximation<sup>67</sup> and chain of spheres (COSX) numerical integration were employed for the HF exchange to speed up the SCF calculations.<sup>68</sup> All SCF calculations used the default tight convergence criteria. In all the cases, the structural models were oriented such that the  $z$  axis was set perpendicular to the approximate  $\text{CoP}_2$  plane, the  $y$  axis aligned with the Co-P bonds and the  $x$  axis with the co-ligand, as shown in ESI Scheme S1.† Additional computational details appear in the ESI.†

### Synthesis

$[\text{Co}(\text{NMes})(^t\text{BuPNP})]$ , **2a**. In a 20 mL scintillation vial, 0.051 g (0.11 mmol) of **1** was dissolved in 10 mL of pentane and cooled to  $-40 \text{ }^\circ\text{C}$ . In a separate vial, 0.018 g (0.12 mmol) of mesityl azide was dissolved in 2 mL pentane and similarly cooled to  $-40 \text{ }^\circ\text{C}$ . Once cold, the solution of azide was added dropwise to that of **1** while stirring accompanied by effervescence from liberated  $\text{N}_2$ . The reaction was allowed to continue stirring at room temperature for 1 h. After this time, the reaction mixture was filtered through a short plug of Celite and the resulting solution evaporated to dryness. The remaining residue was dissolved in a minimal amount of pentane and the solution set aside at  $-40 \text{ }^\circ\text{C}$  for 24 h during which time the

desired compound precipitated as 0.052 g (82%) of olive-green crystals. NMR  $^1\text{H}$  (500 MHz,  $\text{C}_6\text{D}_6$ )  $\delta$  13.98 (4H,  $\text{PCH}_2$ ), 5.1 (36H,  $^t\text{Bu}$ ),  $-49.44$  (2H,  $\text{pyr-CH}$ ).  $\mu_{\text{eff}} = 2.6(2)\mu_{\text{B}}$ . Anal. calcd for  $\text{C}_{31}\text{H}_{53}\text{CoN}_2\text{P}_2$ : C, 64.79; H, 9.30; N, 4.87. Found: C, 65.28; H, 9.44; N, 4.74.

$[\text{Co}(\text{NPh})(^t\text{BuPNP})]$ , **2b**. This compound was prepared in an identical fashion to **2a** starting from 0.053 g (0.11 mmol) of **1** and 0.014 g (0.12 mmol) of phenyl azide. The resultant product precipitated from pentane as 0.050 g (86%) of dark green crystals. NMR  $^1\text{H}$  (500 MHz,  $\text{C}_6\text{D}_6$ )  $\delta$  16.12 (4H,  $\text{PCH}_2$ ), 5.89 (36H,  $^t\text{Bu}$ ),  $-51.77$  (2H,  $\text{pyr-CH}$ ). Anal. calcd for  $\text{C}_{28}\text{H}_{47}\text{CoN}_2\text{P}_2$ : C, 63.15; H, 8.90; N, 5.26. Found: C, 60.74; H, 8.97; N, 5.14. Repeated analyses returned low values for C likely due to the presence of small quantities of **3**.

$[\text{Co}(\text{N}_4\text{Ph}_2)(^t\text{BuPNP})]$ , **3**. In a 20 mL scintillation vial, 0.052 g (0.11 mmol) of **1** was dissolved in 10 mL pentane. In a separate vial, 0.025 g (0.21 mmol) of phenyl azide was dissolved in 3 mL pentane and then added dropwise to the stirring solution of **1** over several minutes. The reaction was allowed to stir for an additional 2 hours after which time it was filtered through a short plug of Celite. The resulting solution was evaporated to dryness and the remaining residue dissolved in a minimal amount of pentane. Cooling of the pentane solution to  $-40$  °C for several days afforded the desired compound as 0.063 g (88%) of olive green crystals. NMR  $^1\text{H}$  (500 MHz,  $\text{C}_6\text{D}_6$ )  $\delta$  11.2 (36H,  $^t\text{Bu}$ ),  $-24.02$  (2H,  $\text{pyr-CH}$ ).  $\mu_{\text{eff}} = 2.9(2)\mu_{\text{B}}$ . Anal. calcd for  $\text{C}_{34}\text{H}_{52}\text{CoN}_5\text{P}_2$ : C, 62.66; H, 8.04; N, 10.75. Found: C, 62.81; H, 7.89; N, 12.22.

$[\text{Co}(\text{NHMe})(^t\text{BuPNP})]$ , **4a**. In a 20 mL scintillation vial, 0.075 g (0.16 mmol) of  $[\text{CoCl}(^t\text{BuPNP})]$  was dissolved in 10 mL of tetrahydrofuran. In a separate vial, 0.024 g (0.17 mmol) of LiNHMe was dissolved in 2 mL of THF. The solution of LiNHMe was added dropwise to the stirring solution of  $[\text{CoCl}(^t\text{BuPNP})]$ , which caused a darkening of the colour. The reaction was allowed to stir for 2 hours at ambient temperature. All volatiles were removed *in vacuo* and the remaining residue was extracted into 10 mL of pentane and filtered through a short Celite plug. The resulting solution was evaporated to dryness to afford the crude material as 0.078 g (90%) of a dark coloured solid. Crystals suitable for diffraction were grown by slow cooling of a saturated pentane solution of the compound at  $-40$  °C. NMR  $^1\text{H}$  (300 MHz,  $\text{C}_6\text{D}_6$ )  $\delta$  30.2 (3H, *p-Me*), 22.0 (2H,  $\text{pyr-CH}$ ), 12.7 (4H,  $\text{PCH}_2$ ), 6.3 (12H, *o-Me*), 3.4 (36H,  $^t\text{Bu}$ ),  $-38.6$  (2H, *m-ArH*).  $\mu_{\text{eff}} = 2.3(2)\mu_{\text{B}}$ . Anal. calcd for  $\text{C}_{31}\text{H}_{54}\text{CoN}_2\text{P}_2$ : C, 64.68; H, 9.46; N, 4.87. Found: C, 62.63; H, 9.61; N, 4.31. Repeated analysis returned low values for C.

$[\text{Co}(\text{NHPh})(^t\text{BuPNP})]$ , **4b**. This compound was prepared in an identical fashion to **4a** starting from 0.100 g (0.21 mmol) of  $[\text{CoCl}(^t\text{BuPNP})]$  and 0.023 g (0.23 mmol) of LiNHPh. After evaporation, the crude material was isolated as 0.123 g (90%) of a purple solid. Crystals suitable for diffraction were grown by slowing cooling a saturated pentane solution of the compound at  $-40$  °C. NMR  $^1\text{H}$  (500 MHz,  $\text{C}_6\text{D}_6$ )  $\delta$  13.9 (4H,  $\text{PCH}_2$ ), 12.27 (2H,  $\text{pyr-CH}$ ), 5.1 (36H,  $^t\text{Bu}$ ),  $-28.2$  (1H, *p-Ph*),  $-44.8$  (2H, *o/m-Ph*),  $-49.7$  (2H, *o/m-Ph*). Anal. calcd for  $\text{C}_{28}\text{H}_{47}\text{CoN}_2\text{P}_2$ : C, 63.15; H, 8.90; N, 5.26. Found: C, 62.66; H, 9.01; N, 5.05.

## General procedure for NMR scale reactions

An NMR tube was charged with 10 mg (0.02 mmol) of the desired cobalt complex and 500  $\mu\text{L}$  of  $\text{C}_6\text{D}_6$ . The H atom donor was then added (1 eq. 0.02 mmol) as a solution in 200  $\mu\text{L}$  of  $\text{C}_6\text{D}_6$ . The reaction mixture was transferred to an NMR tube and spectra were recorded *via* an automated time course every 3 hours over 24 hours.

## Author contributions

The manuscript was written through contributions of all authors. All authors have given approval to the final version of the manuscript.

## Data availability

Crystallographic data for compounds **2a**, **2b**, **3**, **4a**, and **4b** have been deposited at the CCDC under 2334970–2334974.†

## Conflicts of interest

There are no conflicts to declare.

## Acknowledgements

The authors thank the Welch Foundation (AX-1772) for financial support of this work. NMR and X-ray facilities at UTSA were accessed with support from the National Science Foundation (CHE-1625963 and CHE-1920057). Acknowledgement is made to the donors of the American Chemical Society Petroleum Research Fund for support of this research through a DNI grant to SAS (62278-DNI3).

## References

- 1 Y. Park, Y. Kim and S. Chang, Transition Metal-Catalyzed C-H Amination: Scope, Mechanism, and Applications, *Chem. Rev.*, 2017, **117**, 9247–9301.
- 2 J. L. Roizen, M. E. Harvey and J. Du Bois, Metal-Catalyzed, Nitrogen-Atom Transfer Methods for the Oxidation of Aliphatic C-H Bonds, *Acc. Chem. Res.*, 2012, **45**, 911–922.
- 3 J. M. Alderson, J. R. Corbin and J. M. Schomaker, Tunable, Chemo- and Site-Selective Nitrene Transfer Reactions through the Rational Design of Silver(I) Catalysts, *Acc. Chem. Res.*, 2017, **50**, 2147–2158.
- 4 H. J. Lu and X. P. Zhang, Catalytic C-H functionalization by metalloporphyrins: recent developments and future directions, *Chem. Soc. Rev.*, 2011, **40**, 1899–1909.
- 5 C. T. Saouma and J. C. Peters, ME and M=E complexes of iron and cobalt that emphasize three-fold symmetry (EO, N, NR), *Coord. Chem. Rev.*, 2011, **255**, 920–937.

- 6 V. Lyaskovskyy, A. I. O. Suarez, H. J. Lu, H. L. Jiang, X. P. Zhang and B. de Bruin, Mechanism of Cobalt(II) Porphyrin-Catalyzed C-H Amination with Organic Azides: Radical Nature and H-Atom Abstraction Ability of the Key Cobalt(III)-Nitrene Intermediates, *J. Am. Chem. Soc.*, 2011, **133**, 12264–12273.
- 7 Y. Baek, E. T. Hennessy and T. A. Betley, Direct Manipulation of Metal Imido Geometry: Key Principles to Enhance C-H Amination Efficacy, *J. Am. Chem. Soc.*, 2019, **141**, 16944–16953.
- 8 J. F. Berry, Terminal Nitrido and Imido Complexes of the Late Transition Metals, *Comments Inorg. Chem.*, 2009, **30**, 28–66.
- 9 T. Xiong and Q. Zhang, New amination strategies based on nitrogen-centered radical chemistry, *Chem. Soc. Rev.*, 2016, **45**, 3069–3087.
- 10 A. I. O. Suarez, V. Lyaskovskyy, J. N. H. Reek, J. I. van der Vlugt and B. de Bruin, Complexes with Nitrogen-Centered Radical Ligands: Classification, Spectroscopic Features, Reactivity, and Catalytic Applications, *Angew. Chem., Int. Ed.*, 2013, **52**, 12510–12529.
- 11 A. Kalra, V. Bagchi, P. Paraskevopoulou, P. Das, L. Ai, Y. Sanakis, G. Raptopoulos, S. Mohapatra, A. Choudhury, Z. C. Sun, T. R. Cundari and P. Stavropoulos, Is the Electrophilicity of the Metal Nitrene the Sole Predictor of Metal-Mediated Nitrene Transfer to Olefins? Secondary Contributing Factors as Revealed by a Library of High-Spin Co(II) Reagents, *Organometallics*, 2021, **40**, 1974–1996.
- 12 R. E. Cowley, N. A. Eckert, S. Vaddadi, T. M. Figg, T. R. Cundari and P. L. Holland, Selectivity and Mechanism of Hydrogen Atom Transfer by an Isolable Imidoiron(III) Complex, *J. Am. Chem. Soc.*, 2011, **133**, 9796–9811.
- 13 A. Grünwald, S. S. Anjana and D. Munz, Terminal Imido Complexes of the Groups 9–11: Electronic Structure and Developments in the Last Decade, *Eur. J. Inorg. Chem.*, 2021, **2021**, 4147–4166.
- 14 Y. Baek, A. Das, S. L. Zheng, J. H. Reibenspies, D. C. Powers and T. A. Betley, C-H Amination Mediated by Cobalt Organoazide Adducts and the Corresponding Cobalt Nitrenoid Intermediates, *J. Am. Chem. Soc.*, 2020, **142**, 11232–11243.
- 15 Y. Baek and T. A. Betley, Catalytic C-H Amination Mediated by Dipyrrin Cobalt Imidos, *J. Am. Chem. Soc.*, 2019, **141**, 7797–7806.
- 16 Y. Hu, K. Lang, J. R. Tao, M. K. Marshall, Q. G. Cheng, X. Cui, L. Wojtas and X. P. Zhang, Next-Generation -Symmetric Chiral Porphyrins for Cobalt(II)-Based Metalloradical Catalysis: Catalyst Engineering by Distal Bridging, *Angew. Chem., Int. Ed.*, 2019, **58**, 2670–2674.
- 17 H. J. Lu, V. Subbarayan, J. R. Tao and X. P. Zhang, Cobalt (II)-Catalyzed Intermolecular Benzylic C-H Amination with 2,2,2-Trichloroethoxycarbonyl Azide (TroCN), *Organometallics*, 2010, **29**, 389–393.
- 18 V. Bagchi, A. Kalra, P. Das, P. Paraskevopoulou, S. Gorla, L. Ai, Q. W. Wang, S. Mohapatra, A. Choudhury, Z. C. Sun, T. R. Cundari and P. Stavropoulos, Comparative Nitrene-Transfer Chemistry to Olefinic Substrates Mediated by a Library of Anionic Mn(II) Triphenylamido-Amine Reagents and M(II) Congeners (M = Fe, Co, Ni) Favoring Aromatic over Aliphatic Alkenes, *ACS Catal.*, 2018, **8**, 9183–9206.
- 19 L. Capdevila, M. Montilla, O. Planas, A. Brotons, P. Salvador, V. Martin-Diaconescu, T. Parella, J. M. Luis and X. Ribas, C-H Amination Reactions Mediated by Metastable Pseudo-Masked Aryl-Co-nitrene Species, *Inorg. Chem.*, 2022, **61**, 14075–14085.
- 20 Y. Park, S. P. Semproni, H. Y. Zhong and P. J. Chirik, Synthesis, Electronic Structure, and Reactivity of a Planar Four-Coordinate, Cobalt-Imido Complex, *Angew. Chem., Int. Ed.*, 2021, **60**, 14376–14380.
- 21 W. Q. Mao, Z. H. Zhang, D. Fehn, S. A. V. Jannuzzi, F. W. Heinemann, A. Scheurer, M. van Gastel, S. DeBeer, D. Munz and K. Meyer, Synthesis and Reactivity of a Cobalt-Supported Singlet Nitrene, *J. Am. Chem. Soc.*, 2023, **145**, 13650–13662.
- 22 J. Z. Du, L. B. Wang, M. H. Xie and L. Deng, A Two-Coordinate Cobalt(II) Imido Complex with NHC Ligation: Synthesis, Structure, and Reactivity, *Angew. Chem., Int. Ed.*, 2015, **54**, 12640–12644.
- 23 L. Zhang, Y. S. Liu and L. Deng, Three-Coordinate Cobalt (IV) and Cobalt(V) Imido Complexes with N-Heterocyclic Carbene Ligation: Synthesis, Structure, and Their Distinct Reactivity in C-H Bond Amination, *J. Am. Chem. Soc.*, 2014, **136**, 15525–15528.
- 24 X. L. Hu and K. Meyer, Terminal cobalt(III) imido complexes supported by tris(carbene) ligands: Imido insertion into the cobalt-carbene bond, *J. Am. Chem. Soc.*, 2004, **126**, 16322–16323.
- 25 X. L. Dai, P. Kapoor and T. H. Warren, [MeNN]Co( $\eta$ -toluene):: O=O, N=N, and O=N bond cleavage provides,  $\beta$ -diketiminato cobalt  $\mu$ -oxo and imido complexes, *J. Am. Chem. Soc.*, 2004, **126**, 4798–4799.
- 26 E. R. King, G. T. Sazama and T. A. Betley, Co(III) Imidos Exhibiting Spin Crossover and C-H Bond Activation, *J. Am. Chem. Soc.*, 2012, **134**, 17858–17861.
- 27 D. T. Shay, G. P. A. Yap, L. N. Zakharov, A. L. Rheingold and K. H. Theopold, Intramolecular C-H activation by an open-shell cobalt(III) imido complex, *Angew. Chem., Int. Ed.*, 2005, **44**, 1508–1510.
- 28 D. M. Jenkins, T. A. Betley and J. C. Peters, Oxidative group transfer to Co(I) affords a terminal Co(III) imido complex, *J. Am. Chem. Soc.*, 2002, **124**, 11238–11239.
- 29 W. Q. Mao, D. Fehn, F. W. Heinemann, A. Scheurer, M. van Gastel, S. A. V. Jannuzzi, S. DeBeer, D. Munz and K. Meyer, Umpolung in a Pair of Cobalt(III) Terminal Imido/Imidyl Complexes, *Angew. Chem., Int. Ed.*, 2022, **61**, e202206848.
- 30 W. Q. Mao, D. Fehn, F. W. Heinemann, A. Scheurer, D. Munz and K. Meyer, A Pair of Cobalt(III/IV) Terminal Imido Complexes, *Angew. Chem., Int. Ed.*, 2021, **60**, 16480–16486.
- 31 Y. Liu, J. Z. Du and L. Deng, Synthesis, Structure, and Reactivity of Low-Spin Cobalt(II) Imido Complexes [(Me<sub>3</sub>P)<sub>3</sub>Co(NAR)], *Inorg. Chem.*, 2017, **56**, 8278–8286.

- 32 B. Wu, R. H. Sánchez, M. W. Bezpalko, B. M. Foxman and C. M. Thomas, Formation of Heterobimetallic Zirconium/Cobalt Diimido Complexes via a Four-Electron Transformation, *Inorg. Chem.*, 2014, **53**, 10021–10023.
- 33 T. Schmidt-Räntsch, H. Verplancke, J. N. Lienert, S. Demeshko, M. Otte, G. P. Van Trieste, K. A. Reid, J. H. Reibenspies, D. C. Powers, M. C. Holthausen and S. Schneider, Nitrogen Atom Transfer Catalysis by Metallonitrene C-H Insertion: Photocatalytic Amidation of Aldehydes, *Angew. Chem., Int. Ed.*, 2022, **61**, e202115626.
- 34 L. N. Grant, M. E. Carroll, P. J. Carroll and D. J. Mindiola, An Unusual Cobalt Azide Adduct That Produces a Nitrene Species for Carbon-Hydrogen Insertion Chemistry, *Inorg. Chem.*, 2016, **55**, 7997–8002.
- 35 M. J. Ingleson, M. Pink, H. Fan and K. G. Caulton, Redox chemistry of the triplet complex (PNP)Co, *J. Am. Chem. Soc.*, 2008, **130**, 4262–4276.
- 36 V. Vreeken, L. Baij, B. de Bruin, M. A. Siegler and J. I. van der Vlugt, N-Atom transfer thermal or photolytic activation of a Co-azido complex with a PNP pincer ligand, *Dalton Trans.*, 2017, 7145–7149.
- 37 W. A. Chomitz and J. Arnold, Reactivity of a Co(I) [N<sub>2</sub>P<sub>2</sub>] complex with azides:: evidence for a transient Co(III) imido species, *Chem. Commun.*, 2008, 3648–3650.
- 38 J. So, S. Kim, K. B. Cho and Y. Lee, Metal-ligand cooperative transformation of alkyl azide to isocyanate occurring at a Co-Si moiety, *Chem. Commun.*, 2021, **57**, 3219–3222.
- 39 C. V. Thompson and Z. J. Tonzetich, Pincer ligands incorporating pyrrolyl units: Versatile platforms for organometallic chemistry and catalysis, *Adv. Organomet. Chem.*, 2020, **74**, 153–240.
- 40 L. S. Merz, J. Ballmann and L. H. Gade, Phosphines and -Heterocycles Joining Forces: an Emerging Structural Motif in PNP-Pincer Chemistry, *Eur. J. Inorg. Chem.*, 2020, **2020**, 2023–2042.
- 41 H. Alawisi, K. F. Al-Afyouni, H. D. Arman and Z. J. Tonzetich, Aldehyde Decarbonylation by a Cobalt(I) Pincer Complex, *Organometallics*, 2018, **37**, 4128–4135.
- 42 H. Alawisi, H. D. Arman and Z. J. Tonzetich, Catalytic Hydrogenation of Alkenes and Alkynes by a Cobalt Pincer Complex: Evidence of Roles for Both Co(I) and Co(II), *Organometallics*, 2021, **40**, 1062–1070.
- 43 A. L. Amaya, H. Alawisi, H. D. Arman and Z. J. Tonzetich, Well-Defined Cobalt-Silyl Complexes and Their Role in Catalytic Carbonyl Hydrosilylation, *Organometallics*, 2023, **42**, 2902–2909.
- 44 Y. Baek and T. A. Betley, Reversible C-C Bond Cleavage of a Cobalt Diketimide into an Elusive Cobalt Aryl Nitrenoid Complex, *Angew. Chem., Int. Ed.*, 2022, **61**, e202115437.
- 45 G. C. Bai and D. W. Stephan, Formation of C-C and C-N bonds in Ni ketimide complexes via transient Ni aryl imides, *Angew. Chem., Int. Ed.*, 2007, **46**, 1856–1859.
- 46 K. M. Carsch, I. M. DiMucci, D. A. Iovan, A. Li, S. L. Zheng, C. J. Titus, S. J. Lee, K. D. Irwin, D. Nordlund, K. M. Lancaster and T. A. Betley, Synthesis of a copper-supported triplet nitrene complex pertinent to copper-catalyzed amination, *Science*, 2019, **365**, 1138–1143.
- 47 A. Bakhoda, Q. Jiang, J. A. Bertke, T. R. Cundari and T. H. Warren, Elusive Terminal Copper Arylnitrene Intermediates, *Angew. Chem., Int. Ed.*, 2017, **56**, 6426–6430.
- 48 D. S. Moore and S. D. Robinson, Catenated Nitrogen Ligands .1. Transition-Metal Derivatives of Triazenes, Tetrazenes, Tetrazadienes, and Pentazadienes, *Adv. Inorg. Chem. Radiochem.*, 1986, **30**, 1–68.
- 49 A. C. Bowman, A. M. Tondreau, E. Lobkovsky, G. W. Margulieux and P. J. Chirik, Synthesis and Electronic Structure Diversity of Pyridine(diimine)iron Tetrazene Complexes, *Inorg. Chem.*, 2018, **57**, 9634–9643.
- 50 A. Reckziegel, C. Pietzonka, F. Kraus and C. G. Werncke, C-H Bond Activation by an Imido Cobalt(III) and the Resulting Amido Cobalt(II) Complex, *Angew. Chem., Int. Ed.*, 2020, **59**, 8527–8531.
- 51 S. P. Semproni, C. Milsmann and P. J. Chirik, Four-Coordinate Cobalt Pincer Complexes: Electronic Structure Studies and Ligand Modification by Homolytic and Heterolytic Pathways, *J. Am. Chem. Soc.*, 2014, **136**, 9211–9224.
- 52 A. H. Maki, A. Davison, N. Edelstein and R. H. Holm, Electron Paramagnetic Resonance Studies of Electronic Structures of Bis(Maleonitriledithiolato)Copper(2) -Nickel(3) -Cobalt(2) + -Rhodium(2) Complexes, *J. Am. Chem. Soc.*, 1964, **86**, 4580–4587.
- 53 Y. Nishida, A. Sumita and S. Kida, ESR and Optical Spectra of Low-spin Square Planar Cobalt(II) Complexes with Some Quadridentate Schiff Bases of the N<sub>2</sub>S<sub>2</sub> Type, *Bull. Chem. Soc. Jpn.*, 1977, **50**, 759–760.
- 54 Y. Park, S. Kim, L. Tian, H. Y. Zhong, G. D. Scholes and P. J. Chirik, Visible light enables catalytic formation of weak chemical bonds with molecular hydrogen, *Nat. Chem.*, 2021, **13**, 969–976.
- 55 J. J. Zheng, X. F. Xu and D. G. Truhlar, Minimally augmented Karlsruhe basis sets, *Theor. Chem. Acc.*, 2011, **128**, 295–305.
- 56 J. L. Steele, L. Tahsini, C. Sun, J. K. Elinburg, C. M. Kotyk, J. McNeely, S. A. Stoian, A. Dragulescu-Andrasi, A. Ozarowski, M. Ozerov, J. Krzystek, J. Telser, J. W. Bacon, J. A. Golen, A. L. Rheingold and L. H. Doerrer, Square-planar Co(III) in {O<sub>4</sub>} coordination: large ZFS and reactivity with ROS, *Chem. Commun.*, 2018, **54**, 12045–12048.
- 57 V. M. Krishnan, H. D. Arman and Z. J. Tonzetich, Preparation and reactivity of a square-planar PNP cobalt(II)-hydrido complex: isolation of the first {Co-NO}-hydride, *Dalton Trans.*, 2018, 1435–1441.
- 58 S. W. Kwok, J. R. Fotsing, R. J. Fraser, V. O. Rodionov and V. V. Fokin, Transition-Metal-Free Catalytic Synthesis of 1,5-Diaryl-1,2,3-triazoles, *Org. Lett.*, 2010, **12**, 4217–4219.
- 59 *CrysAlisPro*, Rigaku Oxford Diffraction: Rigaku Corporation, The Woodlands, TX, 2015.
- 60 *SCALE3 ABSPACK -An Oxford Diffraction program*, Oxford Diffraction Ltd., 2005.

- 61 O. V. Dolomanov, L. J. Bourhis, R. J. Gildea, J. A. K. Howard and H. Puschmann, OLEX2: a complete structure solution, refinement and analysis program, *J. Appl. Crystallogr.*, 2009, **42**, 339–341.
- 62 G. M. Sheldrick, A short history of SHELX, *Acta Crystallogr., Sect. A: Found. Crystallogr.*, 2008, **64**, 112–122.
- 63 G. Sheldrick, SHELXT - Integrated space-group and crystal-structure determination, *Acta Crystallogr., Sect. A: Found. Adv.*, 2015, **71**, 3–8.
- 64 F. Neese, Software update: The ORCA program system-Version 5.0, *Wiley Interdiscip. Rev.: Comput. Mol. Sci.*, 2022, **12**, e1606.
- 65 F. Neese, F. Wennmohs, U. Becker and C. Riplinger, The ORCA quantum chemistry program package, *J. Chem. Phys.*, 2020, **152**, 224108.
- 66 G. L. Stoychev, A. A. Auer and F. Neese, Automatic Generation of Auxiliary Basis Sets, *J. Chem. Theory Comput.*, 2017, **13**, 554–562.
- 67 F. Neese, An improvement of the resolution of the identity approximation for the formation of the Coulomb matrix, *J. Comput. Chem.*, 2003, **24**, 1740–1747.
- 68 F. Neese, F. Wennmohs, A. Hansen and U. Becker, Efficient, approximate and parallel Hartree-Fock and hybrid DFT calculations. A ‘chain-of-spheres’ algorithm for the Hartree-Fock exchange, *Chem. Phys.*, 2009, **356**, 98–109.